PERGAMON

International Journal of Solids and Structures 37 (2000) 6361–6380

INTERNATIONAL JOURNAL OF SOLIDS and STRUCTURES

www.elsevier.com/locate/ijsolstr

Characteristic state plasticity for granular materials Part II: Model calibration and results

Aylin Ahadi [a], Steen Krenk [b,*]

[a] *Division of Mechanics, Lund Institute of Technology, Box 118, S-221 00 Lund, Sweden*
[b] *Department of Structural Engineering and Materials, Technical University of Denmark, DK-2800 Lyngby, Denmark*

Received 12 May 1999; in revised form 20 September 1999

Abstract

A non-associated plasticity theory for granular materials has been developed in Part 1 based on the concept of a characteristic stress state of vanishing incremental dilation. The model is fully three-dimensional and is defined by six material parameters: two for elastic stiffness, one for plastic stiffness, two for the shapes of yield and plastic potential surfaces and one for the dilation at failure. In this paper a calibration procedure is developed using test data only from a standard triaxial test. It is found that the shape parameter for the yield surface can be estimated from the plastic flow parameters, thus reducing the number of free parameters to five. Calibration examples are shown, as well as predictions made, for different confining stress levels and constant volume tests on sand. The model is found to represent stress–strain behaviour and development of volumetric strain in standard triaxial tests well. The model provides good predictions of constant volume behaviour of dense as well as loose sand on the basis of calibration by standard triaxial test data. A simple explicit formula is derived for the failure asymptote in constant volume testing, enabling explicit adjustment of the parameters, if incompressible test data is available.

Keywords: Plasticity; Granular materials; Soil mechanics

1. Introduction

It is a characteristic of granular materials that the relative motion between the grains leads to irrecoverable deformation, and this suggests the use of plasticity theory as a theoretical framework for the mechanical behaviour of dense granular media. When intergranular friction is the dominating mechanism of deformation, it appears necessary to introduce a non-associated flow rule. Thus, a

* Corresponding author. Tel.: +45-4525-1702; fax: +45-4588-3282.
E-mail address: sk@bkm.dtu.dk (S. Krenk).

0020-7683/00/$ - see front matter
PII: S0020-7683(99)00279-6

plasticity theory suitable for granular materials will include a yield surface, a flow potential, a hardening rule and some representation of elastic deformation. Ideally these properties should be derived from the micromechanical behaviour of the material, but at the present stage most of the properties of a macroscopic elasto-plastic theory for granular materials must be developed on a phenomenological basis.

A notable contribution to the development of constitutive models for granular materials was made by the single hardening model of Lade and Kim (1995). This model makes use of a yield function and a flow potential containing the third stress invariant, hardening and softening rules involving exponentials and non-linear power law elastic relations. In total the model requires 12 material parameters and an independent investigation by Andersen et al. (1997) indicates that proper calibration of the model is essential for its accuracy.

In Part 1 of this study an alternative, somewhat simpler, plasticity theory for friction dominated granular media was developed (Krenk, 1999). The complexity of this model is deliberately reduced to the absolute minimum required to represent a number of essential features. The model appears as a generalization of the classical Cam–Clay model in which a critical surface separates dilative and contractive behaviour (Schofield and Wroth, 1968). In the present model a distinction is made between the characteristic state separating dilative and contractive behaviour, and the ultimate state typically associated with dilation. The model is given representative triaxial features by using a surface format for the yield function and the flow potential that fits smoothly into the compression octant of principal stress space (Krenk, 1996). This format is similar to that of Lade and Kim (1995), but in the present theory the shape of the flow potential is derived from a consistent friction hypothesis, closely resembling a generalized Coulomb friction theory (Krenk, 1998). The hardening is governed by weighted plastic work, in which the work of the deviatoric strains is given a small weight. The elastic theory is deliberately kept in the simple form of the original Cam–Clay theory, i.e. constant shear modulus and tangent bulk modulus proportional to current mean stress. This is justified by the results of the theory, that show little improvement by introducing a more general power law, and also by the simplicity of the relations used in the calibration of the theory as shown in the following.

The resulting theory only involves six parameters, two for shape of yield surface and flow potential, one for dilation at failure, and three stiffness parameters. The present paper deals with the determination of these parameters from standard triaxial test data. In spite of the rather small number of parameters, it turns out that data from a standard triaxial test will leave two of the parameters nearly linearly dependent. This permits a reduction of the number of parameters to be calibrated, to five. A detailed analysis of the model predictions of a constant volume triaxial test demonstrates how supplementary data from such a test can be used to calibrate all six parameters.

The present model captures the essential features of granular materials, as evidenced in triaxial tests, qualitatively as well as quantitatively. In particular the development of volume strain is predicted well. In the concluding part a possible use of an improved elasticity representation and dependence of elastic properties on plastic deformation is discussed.

2. Basic parameters and strategy

2.1. Yield surface and plastic potential

The characteristic state plasticity model developed in Part 1 is formulated in terms of a family of yield surfaces in the form

$$f(\boldsymbol{\sigma}) = -J_3 + pJ_2 - \gamma_f^2(p)p^3 = 0 \tag{1}$$

where $\boldsymbol{\sigma}$ is the stress tensor, J_2, J_3 are the second and third deviatoric stress invariants, and p is the mean stress. Compression is considered positive. The shape of the yield surface defined by Eq. (1) is specified via the function $\gamma_f(p)$. A closed surface with drop shape that fits into the compression octant in principal stress space is obtained by selecting the function as

$$\gamma_f(p)^2 = 1 - \left(\frac{p}{p_f}\right)^m \tag{2}$$

where $p = p_f$ is the intersection with the hydrostatic axis in stress space, and m controls the width of the surface. A typical yield surface is shown in Fig. 1(a).

The plastic potential is assumed to be associated in the deviatoric stress plane, leading to a similar functional form of the flow potential,

$$g(\boldsymbol{\sigma}) = -J_3 + pJ_2 - \gamma_g^2(p)p^3 \tag{3}$$

The shape of the flow potential surfaces is determined by the function $\gamma_g(p)$, and an approximate friction hypothesis proposed in Part 1 leads to the form

$$\gamma_g(p) = 1 - \left(\frac{p}{p_g}\right)^n \tag{4}$$

A typical flow potential surface is shown in Fig. 1(b). The parameter $2n$ represents the intergranular coefficient of friction. It is important to note the difference in shape, caused by the power two in the definition of $\gamma_f(p)$. In the following it is convenient to use the notation $\eta = 1 - \gamma^2$.

Most experimental data is available as results from standard triaxial tests, using a cylindrical test specimen. The test starts by establishing a state of isotropic stress $\sigma_1 = \sigma_2 = \sigma_3$ and then the axial stress component σ_1 is increased, while the transverse components $\sigma_2 = \sigma_3$ are kept constant. The following

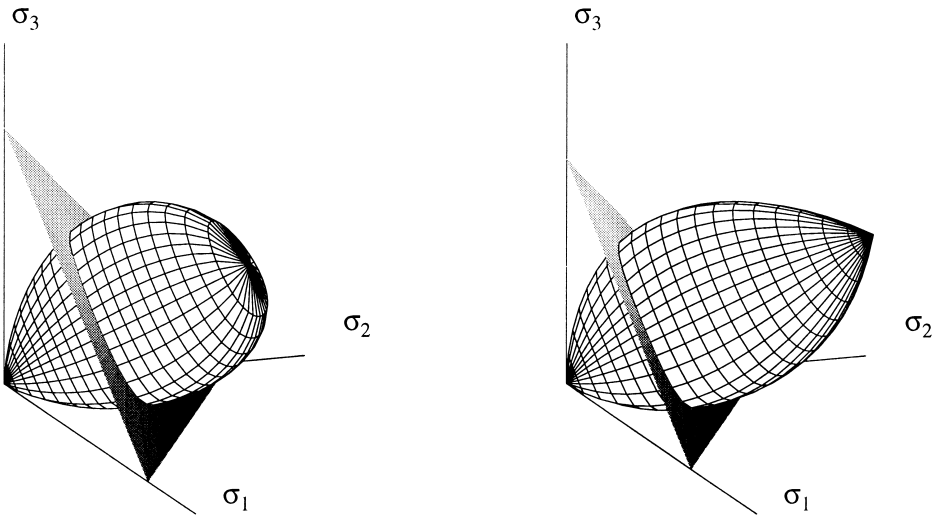

Fig. 1. Principal stress space: a) yield surface, b) flow potential.

calibration procedure is based on this type of data. For convenience a two-dimensional stress space representation is used with mean stress and stress difference defined as

$$p = \frac{1}{3}\sigma_1 + \frac{2}{3}\sigma_3, \qquad q = \sigma_1 - \sigma_3 \tag{5}$$

In terms of the stress components (p, q) the yield surface and flow potential are

$$f(p, q) = -\frac{2}{27}q^3 + \frac{1}{3}q^2 p - \gamma_f^2(p)p^3 \tag{6}$$

$$g(p, q) = -\frac{2}{27}q^3 + \frac{1}{3}q^2 p - \gamma_g^2(p)p^3 \tag{7}$$

In this notation $q > 0$ corresponds to triaxial compression and $q < 0$ to triaxial tension.

2.2. Elastic relations

The strain components corresponding to the stress components (p, q) are

$$\varepsilon_v = \varepsilon_1 + 2\varepsilon_3 \qquad \varepsilon_q = \frac{2}{3}(\varepsilon_1 - \varepsilon_3) \tag{8}$$

The incremental elasticity relation is assumed to be isotropic,

$$\begin{bmatrix} d\varepsilon_v \\ d\varepsilon_q \end{bmatrix} = \begin{bmatrix} K_e^{-1} & \\ & (3G)^{-1} \end{bmatrix} \begin{bmatrix} dp \\ dq \end{bmatrix} \tag{9}$$

where K_e is the tangent elastic bulk modulus, and G is the tangent elastic shear modulus. The elements of the tangent flexibility matrix in the incremental elasticity relation Eq. (9) are the second partial derivatives of the complementary elastic energy density.

Several authors have used power laws to describe the dependence of the elastic properties on the current state of stress. A common procedure, described e.g. by Lade and Nelson (1987), is to assume that the complementary elastic energy is a power function of the isotropic stress invariant

$$I_\beta = \frac{1}{2}p^2 + \beta J_2 = \frac{1}{2}p^2 + \frac{1}{3}\beta q^2 \tag{10}$$

where β is a material parameter, specifying the Poisson ratio. It is easily verified by differentiation that if the complementary elastic energy is a non-linear function $U_c(I_\beta)$, the *secant* flexibility is isotropic, while further differentiation leads to coupling terms in the *tangent* flexibility. Thus, the assumption of a complementary elastic energy in the form $U_c(I_\beta)$ implies stress dependent anisotropy of the tangent stiffness. The stiffness relations corresponding to an arbitrary complementary energy function $U_c(I_\beta)$ are easily calculated, but in the present "minimal model" an uncoupled form with constant shear modulus G and tangent elastic bulk modulus

$$K_e = \frac{p}{\kappa} \tag{11}$$

has been selected. There are two reasons for this choice. First, the elastic parameters are expected to depend on the state of the material, including e.g. changes in pore volume due to plastic straining. This

effect is not captured by introducing a power law format in accordance with Eq. (10). Secondly, the uncoupled format Eq. (9) leads to simple explicit results for the direction of the initial strain increment of a standard triaxial test and for the ratio of the stresses in a constant volume test. As demonstrated below, these results are quite useful in the calibration procedure and the accuracy of the results indicate the practical usefulness of the model in its present form.

2.3. Hardening rule

The direction of the plastic strain increments is given by the gradient of the flow potential, while the magnitude is determined implicitly by a multiplier $\mathrm{d}\chi$,

$$\begin{bmatrix} \mathrm{d}\varepsilon_{\mathrm{v}}^{\mathrm{p}} \\ \mathrm{d}\varepsilon_{\mathrm{q}}^{\mathrm{p}} \end{bmatrix} = \mathrm{d}\chi \begin{bmatrix} \partial g/\partial p \\ \partial g/\partial q \end{bmatrix} \tag{12}$$

The hardening parameter $H = \partial f/\partial \chi$ determines the change of the yield function per unit change of the plastic multiplier χ. In the present model the change of the yield function is determined by the size parameter p_{f} and thus

$$H = -\frac{\partial f}{\partial p_{\mathrm{f}}}\frac{\mathrm{d}p_{\mathrm{f}}}{\mathrm{d}\chi} = H_1 H_2 \tag{13}$$

The factor H_1 follows from differentiation of the yield function Eq. (6), using the particular form Eq. (2) of the shape function $\gamma_{\mathrm{f}}(p)^2$.

$$H_1 = -\frac{\partial f}{\partial p_{\mathrm{f}}} = mp^2\left(1-\gamma_{\mathrm{f}}^2\right)^{(m+1)/m} \tag{14}$$

where the value of γ_{f}^2 is expressed in terms of the current stress state by use of the yield condition Eq. (6).

It is convenient to specify the plastic hardening with reference to isotropic compression. The total strain is the sum of an elastic and plastic part, and thus in isotropic compression the following relations define the elastic, plastic and elasto-plastic bulk moduli K_{e}, K_{p} and K_{ep},

$$\frac{\mathrm{d}\varepsilon_{\mathrm{v}}^{\mathrm{e}}}{\mathrm{d}p} + \frac{\mathrm{d}\varepsilon_{\mathrm{v}}^{\mathrm{p}}}{\mathrm{d}p} = \frac{\mathrm{d}\varepsilon_{\mathrm{v}}}{\mathrm{d}p} \qquad \frac{1}{K_{\mathrm{e}}} + \frac{1}{K_{\mathrm{p}}} = \frac{1}{K_{\mathrm{ep}}} \tag{15}$$

The elasto-plastic bulk modulus K_{ep} is assumed in the form

$$K_{\mathrm{ep}} = \frac{p}{\lambda} \tag{16}$$

similar to Eq. (11) with the non-dimensional elasto-plastic flexibility parameter λ.

A suitable hardening rule is obtained by generalizing the isotropic elasto-plastic compression relation

$$\mathrm{d}p_{\mathrm{f}} = \mathrm{d}p = K_{\mathrm{p}}\mathrm{d}\varepsilon_{\mathrm{v}}^{\mathrm{p}} \tag{17}$$

A contribution of the work via the plastic deviatoric strains with weight w is added and after introducing the plastic strain increments from Eq. (12), the hardening factorH_2 is obtained in the form

$$H_2 = \frac{\mathrm{d}p_{\mathrm{f}}}{\mathrm{d}\chi} = K_{\mathrm{p}}\left(\frac{\partial g}{\partial p} + w\frac{q}{p}\frac{\partial g}{\partial q}\right) \tag{18}$$

The non-dimensional weight w controls the dilation in the ultimate state, where $H_2 = 0$.In the present p, q format the incremental elasto-plastic stiffness equations take the following matrix form

$$\begin{bmatrix} \mathrm{d}p \\ \mathrm{d}q \end{bmatrix} = \left(\begin{bmatrix} K_\mathrm{e} & \\ & 3G \end{bmatrix} - \frac{\begin{bmatrix} K_\mathrm{e}\partial g/\partial p \\ 3G\partial g/\partial q \end{bmatrix} \begin{bmatrix} K_\mathrm{e}\dfrac{\partial f}{\partial p}, & 3G\dfrac{\partial f}{\partial q} \end{bmatrix}}{H + \dfrac{\partial g}{\partial p}K_\mathrm{e}\dfrac{\partial f}{\partial p} + \dfrac{\partial g}{\partial q}3G\dfrac{\partial f}{\partial q}} \right) \begin{bmatrix} \mathrm{d}\varepsilon_\mathrm{v} \\ \mathrm{d}\varepsilon_\mathrm{q} \end{bmatrix} \tag{19}$$

These equations are used to calibrate the model from triaxial test data.

2.4. Calibration strategy

The model requires only six parameters: elastic stiffnesses G and κ, elasto-plastic stiffness λ, exponents m and n defining the shape of the yield and plastic potential surfaces and the non-dimensional weight parameter w for the dilation at failure. In the calibration procedure it is convenient to represent the shape parameters m and n by the stress ratios $(q/p)_\mathrm{f} = M_\mathrm{f}$ and $(q/p)_\mathrm{c} = M_\mathrm{c}$, representing the point of maximum width of the yield surface and potential surface, respectively. As shown in Part 1, the yield surface exponent m can be evaluated as

$$m = \frac{6M_\mathrm{f}^2}{(3 - M_\mathrm{f})(3 + 2M_\mathrm{f})} \tag{20}$$

and the flow potential exponent n can be evaluated from

$$n = \frac{1}{9}\frac{M_\mathrm{c}^2(3 - M_\mathrm{c})}{\gamma_\mathrm{c}(1 - \gamma_\mathrm{c})} \qquad \gamma_\mathrm{c}^2 = \frac{1}{3}M_\mathrm{c}^2\left(1 - \frac{2}{9}M_\mathrm{c}\right) \tag{21}$$

The parameter w is related to the behaviour at the ultimate state, corresponding to the stress ratio $(q/p)_\mathrm{u} = M_\mathrm{u}$.

Fig. 2 shows typical results of a triaxial test on sand in the form of plots of the stress ratio q/p and the volumetric strain ε_v vs. the shear strain ε_q. Typically the volumetric strain curve starts out at a finite

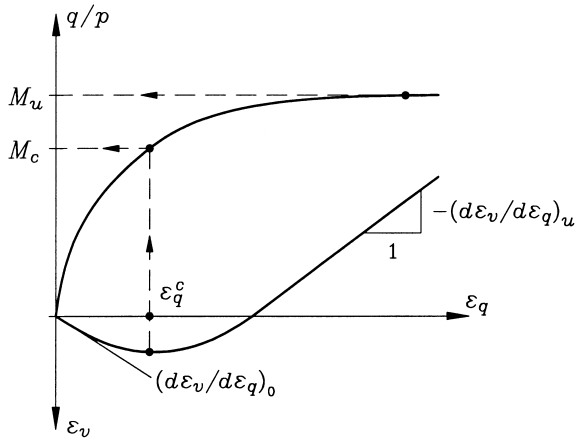

Fig. 2. Normalized stress and volumetric strain vs. shear strain.

positive slope corresponding to compaction, passes through a maximum at the characteristic state, and then turns into dilation. Characteristic features of the $(\varepsilon_v, \varepsilon_q)$ curve are: the initial slope $(d\varepsilon_v/d\varepsilon_q)_0$, the location $(\varepsilon_v^c, \varepsilon_q^c)$ of the maximum, and the slope $(d\varepsilon_v/d\varepsilon_q)_u$ and position of the final part of the dilation curve. The stress curve shows directly the characteristic stress ratio M_c, corresponding to ε_q^c determined from the strain curve, and the ultimate stress ratio M_u, corresponding to the maximum of the curve. These curves suggest that the parameters M_c and M_u are determined first, while the stiffness parameters are determined to match the initial slopes of the stress–strain curves and the location of the final, nearly linear, part of the dilation curve.

In this process there is no direct means of determining the yield surface parameter M_f, which turns out to be nearly linearly dependent of the elastic flexibility κ. Results on measured yield surfaces and analysis of several different data sets suggest that M_f can be estimated from the parameters M_c and M_u, whereby only five material parameters are estimated directly from the test data.

3. The shape parameters M_c, M_u and M_f

The shape parameters M_c, M_u and M_f specify the plastic effects in model. When plastic strains are assumed to dominate around the characteristic and ultimate states, the characteristic and ultimate state lines M_c and M_u can be determined directly from the experimental data curves. The yield function parameter is then estimated from the parameters M_c and M_u.

3.1. Characteristic state parameter M_c

At the characteristic state the volumetric strain increment vanishes, $d\varepsilon_v = 0$. The corresponding value of the strain ε_q^c can be read directly from a graph like Fig. 2 of the volumetric strain, and the corresponding stress ratio $(q/p)_c$ determines M_c. In the theory the term "characteristic state" has been used to denote the state in which the plastic volumetric strain increment vanishes, i.e. $d\varepsilon_v^p = 0$. It is assumed that the plastic strains dominate around the characteristic state and that no correction is therefore needed. This assumption is confirmed by the analysis of experimental data for sand presented in Sections 5 and 6. When M_c has been obtained from the data, the exponent n is calculated from Eq. (21).

3.2. Ultimate state parameter M_u

In the ultimate state the hardening parameter $H = H_1 H_2$ vanishes. When the ultimate stress ratio M_u is inserted into the expression (18) for the factor H_2 an expression for the parameter w in terms of M_u is obtained

$$w = -\frac{p}{q}\frac{\partial g/\partial p}{\partial g/\partial q} = 1 - \frac{n(M_c)}{n(M_u)} \tag{22}$$

where $n(M)$ denotes the value of n given by Eq. (21) for the stress ratio M. $n(M_c)$ is the flow potential exponent already calculated from the characteristic state parameter M_c.

The condition (22) also determines the ratio between the plastic strain increments at the ultimate state, when introducing the plastic strain increment relation (12).

$$\left.\frac{d\varepsilon_v^p}{d\varepsilon_q^p}\right|_u = -wM_u \tag{23}$$

Thus, the parameter w is seen to play a double role in defining the ultimate stress ratio $(q/p)_u = M_u$ and the plastic strain ratio $(d\varepsilon_v^p/d\varepsilon_q^p)_u$ in the ultimate state.

In practice calibration based on the ultimate plastic strain ratio turns out to be considerably more robust and reliable than reading M_u directly from the stress data. Thus, the stress ratio M_u is calculated by solving the nonlinear equation

$$M_u\left(1-\frac{n(M_c)}{n(M_u)}\right)=-\left.\frac{d\varepsilon_v}{d\varepsilon_q}\right|_u \tag{24}$$

obtained by combining Eqs. (22) and (23). Again it is assumed that the slope of the total strain curve is representative of the plastic strains.

3.3. Yield surface shape parameter M_f

The parameter M_f, controlling the shape of the yield surface, is not directly observable in a single triaxial test. The shape of the yield surface is difficult to measure, because any elasto-plastic loading changes the location of the yield surface. The procedure therefore is to introduce elastic unloading from a point on the yield surface, move to a different point inside the yield surface and reload to a new intersection with the yield surface. This procedure produces pairs of stress points on each yield surface. The results of such an experiment on sand by Andersen et al. (1997) are shown in Fig. 3. The figure shows the direction of estimated plastic strain and corresponding segments of the yield surface. It is seen how the direction of the plastic strain increment vector $(d\varepsilon_v^p, d\varepsilon_q^p)$ turns to the left for stress locations with increasing ratio $M = q/p$. The vertical direction of the strain increment identifies the characteristic state $M_c = (q/p)_c$. It is seen that around the characteristic state, where the flow potential has a horizontal tangent, the tangent to the yield surface has an upward slope. The parameters M_c and M_f represent the slope of a line connecting origo with the maximum of the flow potential and the yield surface, respectively, and thus the figure indicates that $M_f < M_c$.

The precise value of M_f is difficult to estimate from the data of standard triaxial tests. The reason is illustrated in Figs. 4 and 5 showing test data of loose Baskarp sand with void ratio $e = 0.85$ and initial hydrostatic stress $p_0 = 985$ kPa. The test data are well represented by the present model with parameters $M_f = 1.00$, $\kappa = 7.5 \times 10^{-3}$ and the other parameters as given in Table 1. Fig. 4 shows the effect of

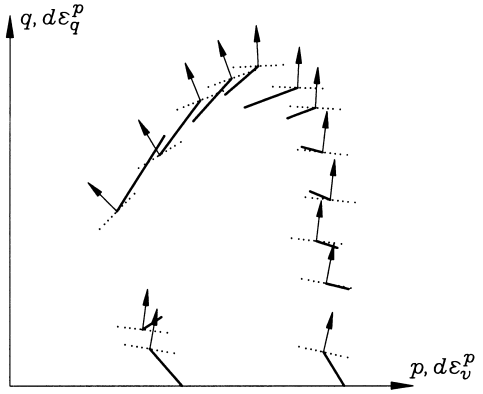

Fig. 3. Direction of plastic strain increments $(d\varepsilon_v^p, d\varepsilon_q^p)$ for Baskarp Sand (Andersen et al., 1997).

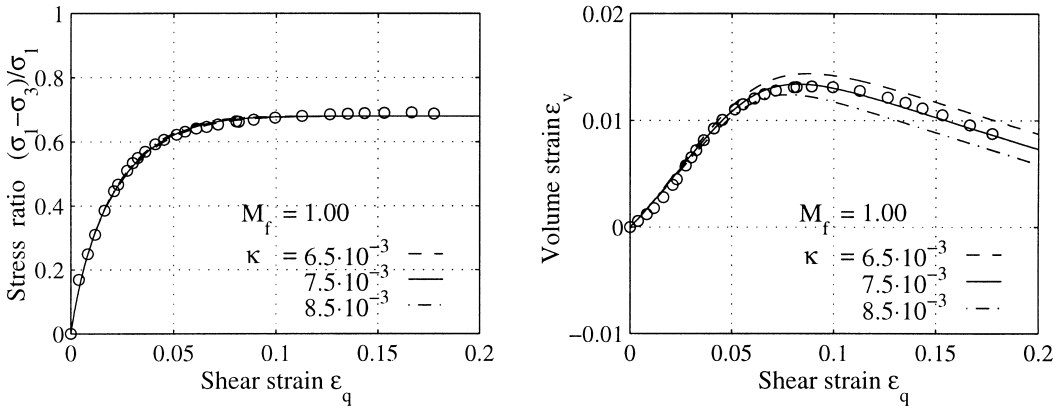

Fig. 4. Variation of the $(\varepsilon_q, \varepsilon_v)$ curve with κ.

increasing and decreasing the parameter κ with $\pm 10^{-3}$. There is virtually no effect on the stress curve, while a decrease of κ moves the dilative part of the strain curve upward. Precisely the same effect can be obtained by keeping the original value $\kappa = 7.5 \times 10^{-3}$ fixed, while changing the value of M_f by ± 0.05 as shown in Fig. 5. Thus, if the parameters M_f and κ in the present case are changed such that $\Delta M_f \simeq -50\Delta\kappa$, there would be no detectable change in the representation of the triaxial test data. A robust calibration procedure must therefore estimate one of the parameters M_f or κ independently, or include additional data, e.g. from a constant volume test as discussed in Section 6.

Analysis of several data sets for sand has indicated that M_f can be estimated from two requirements. For loose packing M_u is close to M_c and this also seems to imply that M_f is close to M_c. In addition the magnitude M_f must be limited e.g. by $M_f < 1$, in order to lead to suitable flexibility parameters κ and λ. A simple estimate for M_f in accordance with these requirements is

$$M_f = \min(1, 2M_c - M_u) \tag{25}$$

This relation has been used in the model calibrations in Sections 5 and 6. In Section 6 is demonstrated

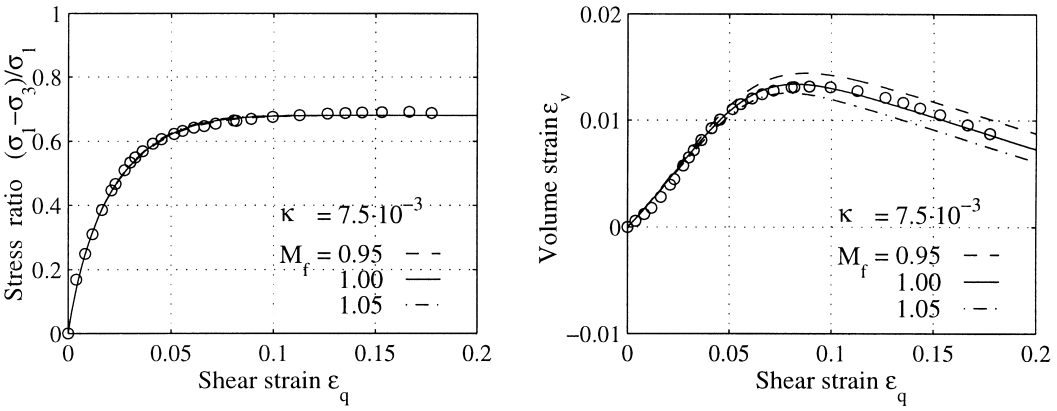

Fig. 5. Variation of the $(\varepsilon_q, \varepsilon_v)$ curve with M_f.

Table 1
Material parameters for loose Baskarp sand, $e = 0.85$

p_0 (kPa)	G (MPa)	$\kappa \times 10^3$	$\lambda \times 10^2$	M_c	M_u	M_f
640	12.0	5.59	1.13	1.201	1.247	1.0
800	12.9	6.03	1.21	1.209	1.252	1.0
985	13.7	7.36	1.37	1.210	1.245	1.0
mean	12.9	6.33	1.24	1.207	1.248	1.0

how the elastic flexibility parameter κ can be evaluated independently from incompressible triaxial test data.

4. The stiffness parameters κ, λ and G

Three conditions are needed to determine the stiffness parameters κ, λ and G. Two equations are obtained by matching the initial elasto-plastic stiffness, i.e. the slope of the stress–strain curves at $q = 0$. In the present model the elasto-plastic volumetric and shear stiffness for the first load increment from an isotropic stress state can be evaluated explicitly, as shown below. The final condition is the position of the asymptote of the $(\varepsilon_v, \varepsilon_q)$ curve. This is the only condition that requires integration of the incremental elasto-plastic stress–strain relations (Eq. (19)).

4.1. Initial elasto-plastic stiffness

In the present theory it is assumed that the yield function $f(\boldsymbol{\sigma})$ is smooth, while it follows from the friction hypothesis of Part 1 that the flow potential has an apex at the hydrostatic axis. These two properties, illustrated in Fig. 6, lead to simple analytical expressions for the strain increments at the first deviation from hydrostatic stress. In the hydrostatic part of the test the plastic strains are a combination of contributions along the normals to the plastic potential at the apex, leading to hydrostatic compression during hardening, according to the argument in Krenk (1998).

At the hydrostatic axis $q = 0$, and as seen from Fig. 6 symmetry and the smooth variation of the yield function imply $\partial f/\partial q = 0$. These conditions lead to particularly simple expressions for the hardening parameters H_1 and H_2 on the hydrostatic axis, namely

$$H_1 = -\frac{\partial f}{\partial p_f} = \frac{\partial f}{\partial p} \qquad H_2 = K_p \frac{\partial g}{\partial p} \tag{26}$$

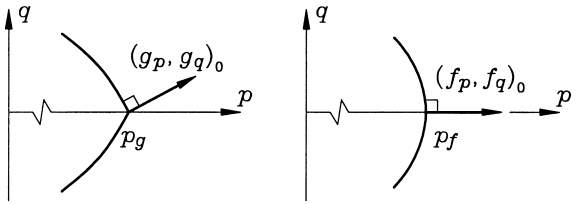

Fig. 6. Flow potential $g(p, q)$ and yield surface $f(p, q)$ at hydrostatic axis.

When these conditions are inserted into the elasto-plastic stress increment formula (19), the following much simpler form is obtained

$$\begin{bmatrix} \mathrm{d}p \\ \mathrm{d}q \end{bmatrix} = \begin{bmatrix} K_{\mathrm{ep}} & 0 \\ \dfrac{\partial g/\partial q}{\partial g/\partial p}\dfrac{3G}{K_{\mathrm{p}}}K_{\mathrm{ep}} & 3G \end{bmatrix} \begin{bmatrix} \mathrm{d}\varepsilon_{\mathrm{v}} \\ \mathrm{d}\varepsilon_{\mathrm{q}} \end{bmatrix} \tag{27}$$

It is clearly seen from this relation, that the apex of the flow potential leads to a coupling between volumetric and shear behaviour right from the start of a triaxial test.

The magnitude of the coupling is determined by the angle at the apex. The ratio between the two partial derivatives at $q = 0$ is determined by expanding the potential $g(p, q)$ around the point $(p_{\mathrm{g}}, 0)$. In this expansion $p = p_{\mathrm{g}} + \Delta p$, and

$$\gamma_{\mathrm{g}}(p) = \left[1 - \left(\frac{p_{\mathrm{g}} + \Delta p}{p_{\mathrm{g}}}\right)^{n}\right] \simeq -n\frac{\Delta p}{p_{\mathrm{g}}} \tag{28}$$

When this expansion is inserted into the flow potential Eq. (7), the following equation is obtained

$$g(p, q) \simeq -\frac{2}{27}q^3 + \frac{1}{3}q^2 p - \left(n\frac{\Delta p}{p_{\mathrm{g}}}\right)^2 p^3 = 0 \tag{29}$$

Retaining only quadratic terms in q and Δp gives the direction of the constant potential curve at $(p_{\mathrm{g}}, 0)$ as

$$q = -\sqrt{3}n\Delta p \tag{30}$$

This direction determines the ratio

$$\left.\frac{\partial g/\partial q}{\partial g/\partial p}\right|_{q=0} = -\left.\frac{\Delta p}{q}\right|_{q=0} = \frac{1}{\sqrt{3}n} \tag{31}$$

This gives a simplified form of the initial stress increment formula (27) for the particular form of the flow potential,

$$\begin{bmatrix} \mathrm{d}p \\ \mathrm{d}q \end{bmatrix} = \begin{bmatrix} K_{\mathrm{ep}} & 0 \\ -\dfrac{\sqrt{3}G}{nK_{\mathrm{p}}}K_{\mathrm{ep}} & 3G \end{bmatrix} \begin{bmatrix} \mathrm{d}\varepsilon_{\mathrm{v}} \\ \mathrm{d}\varepsilon_{\mathrm{q}} \end{bmatrix} \tag{32}$$

It is seen that the relative magnitude of the coupling term is determined by $(\sqrt{3}nK_{\mathrm{p}})^{-1}$.

In a standard triaxial test the non-isotropic stress increments satisfy the relation $\mathrm{d}q = 3\mathrm{d}p$. Thus, the initial non-isotropic strain increments are given by

$$\frac{\mathrm{d}\varepsilon_{\mathrm{v}}}{\mathrm{d}p} = \left(\frac{1}{K_{\mathrm{e}}} + \frac{1}{K_{\mathrm{p}}}\right) = \frac{1}{K_{\mathrm{ep}}} \tag{33a}$$

$$\frac{\mathrm{d}\varepsilon_{\mathrm{q}}}{\mathrm{d}q} = \frac{1}{3}\left(\frac{1}{G} + \frac{1}{K_{\mathrm{p}}}\frac{1}{\sqrt{3}n}\right) \tag{33b}$$

It is seen that the effect of the apex of the flow potential is to produce a plastic contribution to the shear strain increment $d\varepsilon_q$. Test data like Fig. 3, e.g. from Borup and Hedegaard (1995) and Ibsen and Jakobsen (1996), support the existence of a plastic strain contribution to ε_q right from the start of the non-isotropic part of the test.

The relation (33a) determines the parameter λ explicitly, while the relation (33b) is used to calculate G from an assumed value of κ.

4.2. Elastic stiffness parameter κ

The remaining elastic stiffness parameter κ is determined by fitting the final, almost linear, part of the dilation curve (ε_q, ε_v). It is seen from Fig. 4(b), that changes in κ leads to a parallel shift of the final part of the dilation curve. This shift is only moderately affected by the shear modulus and thus correction of κ followed by recalculation of G from Eq. (33b) rapidly leads to convergence.

5. Analysis of standard triaxial tests on sand

The ability of the model to represent standard triaxial test data has been investigated for loose and dense sand, tested at various initial mean stress levels. The experiments were conducted on loose Baskarp sand with void ratio $e = 0.85$ (Borup and Hedegaard, 1995) and dense Lund sand with void ratio $e = 0.57$ (Ibsen and Jakobsen, 1996). The height of the test specimens was equal to the diameter, thus preventing localized failure near the peak load.

The results for loose sand are shown in Fig. 7 and the parameter values are given in Table 1. The top part of the figure shows the theoretical results obtained by calibrating the parameters for each of the three tests. The fit is seen to be excellent. The characteristic state parameter $M_c \simeq 1.2$ with minimal variation. The ultimate state parameter $M_u \simeq 1.25$ is only slightly larger, indicating small additional capacity beyond the characteristic state for loose materials. Also M_u shows very little dependence on initial stress p_0. The yield surface parameter$M_f = 1$ is determined by the restriction on magnitude due to the closeness of M_c and M_u. There is a somewhat larger change in the stiffness parameters, in particular the elastic bulk parameter κ.

The lower part of Fig. 7 shows the theoretical predictions when using one common set of mean value parameters for all three tests. The stress results are still very good, but the use of a common value for κ reduces the experimentally obtained difference between the dilation curves. The results are still quite acceptable from an application point of view. However, the parameters indicate that the shear modulus G should increase slightly with mean stress, while increase of bulk stiffness with mean stress should be somewhat less than linear.

Table 2
Material parameters for dense Lund sand, $e = 0.57$

p_0 (kPa)	G (MPa)	$\kappa \times 10^3$	$\lambda \times 10^3$	M_c	M_u	M_f
40	15.2	2.50	3.16	1.17	1.57	0.77
80	24.3	2.33	3.53	1.22	1.60	0.84
160	21.0	5.92	6.63	1.16	1.53	0.79
320	28.1	5.66	6.96	1.11	1.43	0.79
640	47.3	6.09	7.59	1.13	1.39	0.87
mean	27.2	4.50	5.57	1.16	1.50	0.82

The results for dense sand are shown in Fig. 8 with the corresponding parameters given in Table 2. The range of the initial mean stress level p_0 is much larger than the variation of the parameter values. Also in this case the fit based on individual calibration of each test is excellent. The characteristic state parameter M_c is still around 1.2, but typically for a dense material the ultimate state parameter M_u is now somewhat higher, around 1.5. This implies that the yield parameter M_f is now determined by the relation $M_f = 2M_c - M_u$. Also in this case it is clear that the shear modulus G shows an increase with mean pressure level, while the increase in bulk stiffness with mean stress is less than linear. It is interesting to observe that calibration of the weight parameter w in the hardening rule from the individual dilation curves in the upper part of Fig. 8 leads to correct differentiation of the ultimate stress parameter M_u for the individual tests, although a perfect fit is not obtained.

6. Prediction of constant volume behaviour of sand

The previous section demonstrated the ability of the model to represent the results of standard triaxial tests. This is a prerequisite for ability to predict the stress–strain behaviour under different types of loading. Experimental data is available for standard (drained) well as constant volume (undrained)

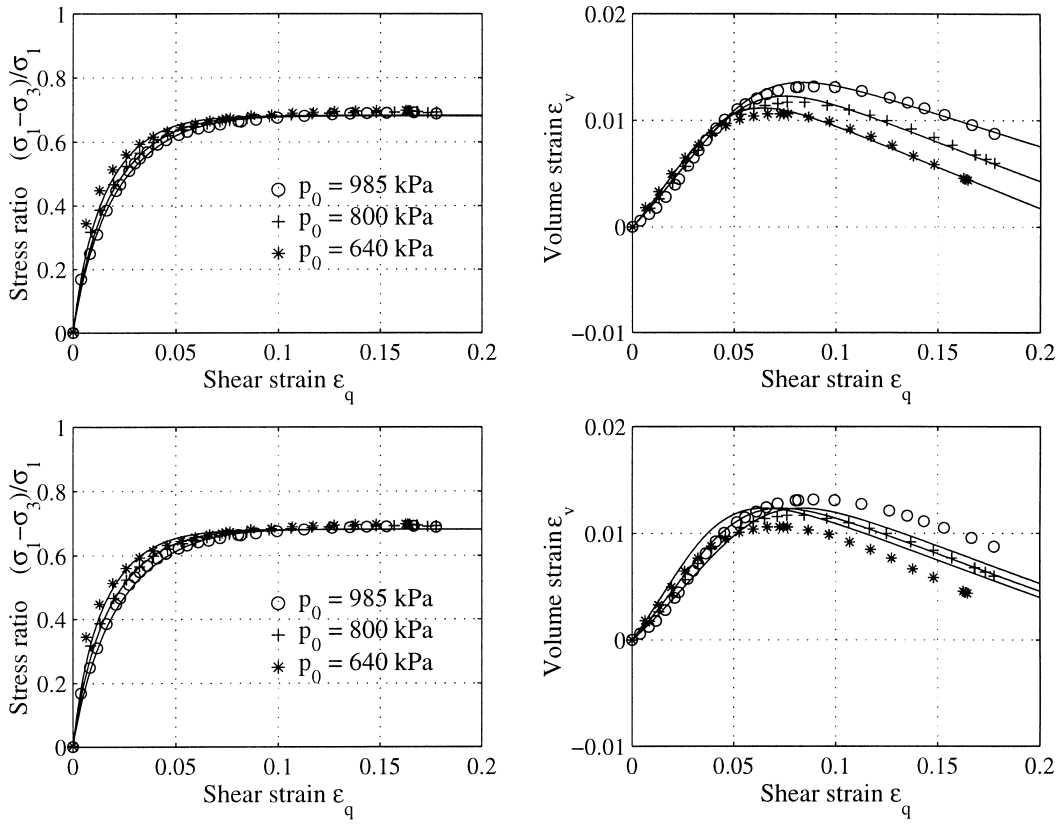

Fig. 7. Theoretical and experimental stress ratio and volumetric strain, loose Baskarp sand. Individual calibration (top) and mean values (bottom).

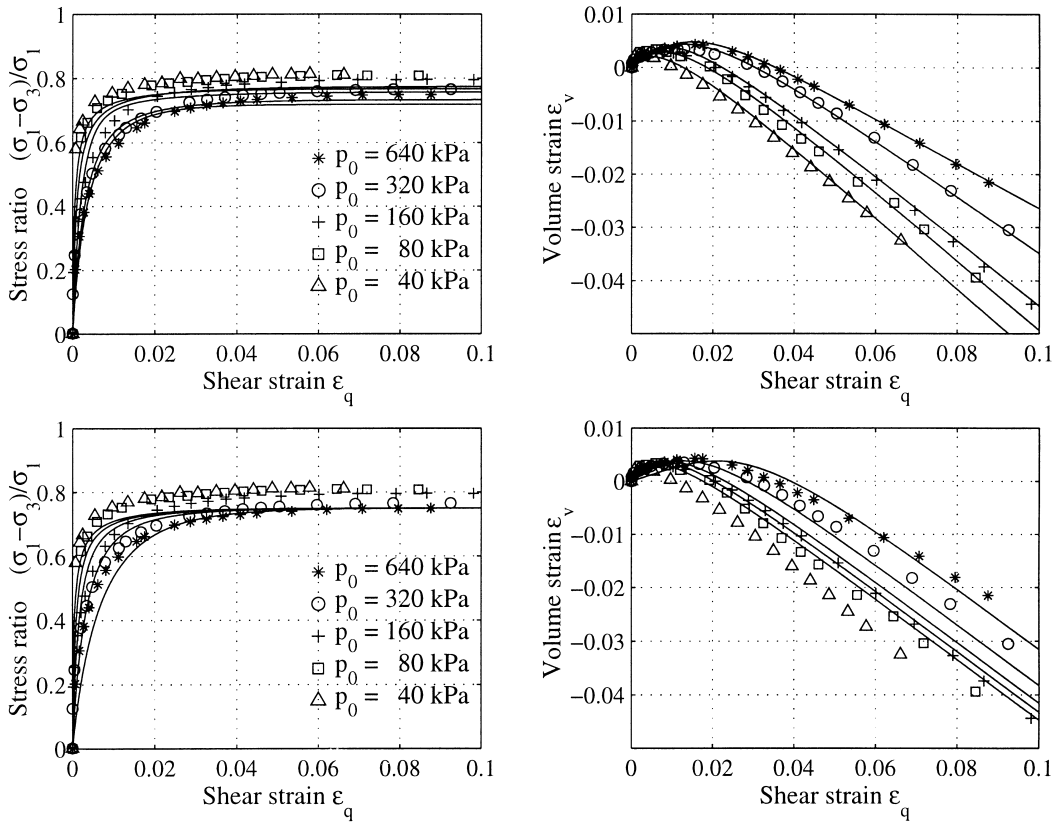

Fig. 8. Theoretical and experimental stress ratio and volumetric strain, dense Lund sand. Individual calibration (top) and mean values (bottom).

triaxial tests on loose and dense Sacramento river sand (Lee and Seed, 1967a, 1967b). The length of the test specimens was greater than the diameter and the behaviour after reaching the maximum stress may, therefore, be influenced by localized failures not accounted for in the theory. Experimental and theoretical results for standard triaxial tests are shown in Fig. 9, and the corresponding parameters are given in Tables 3 and 4. For loose sand only the curve with $p_0 = 0.44$ MPa shows dilation, and for the

Table 3
Material parameters for loose Sacramento sand, $e = 0.87$

p_0 (MPa)	G (MPa)	$\kappa \times 10^3$	$\lambda \times 10^2$	M_c	M_u	M_f
0.44	11.5	0.43	0.64	1.35	1.36	1.0
1.24	43.7	0.64	2.41	1.33	1.33	1.0
1.96	61.8	1.39	3.58	1.38	1.38	1.0
3.93	108.2	6.63	5.78	1.37	1.37	1.0
mean	56.3	4.30	5.70	1.35	1.36	1.0

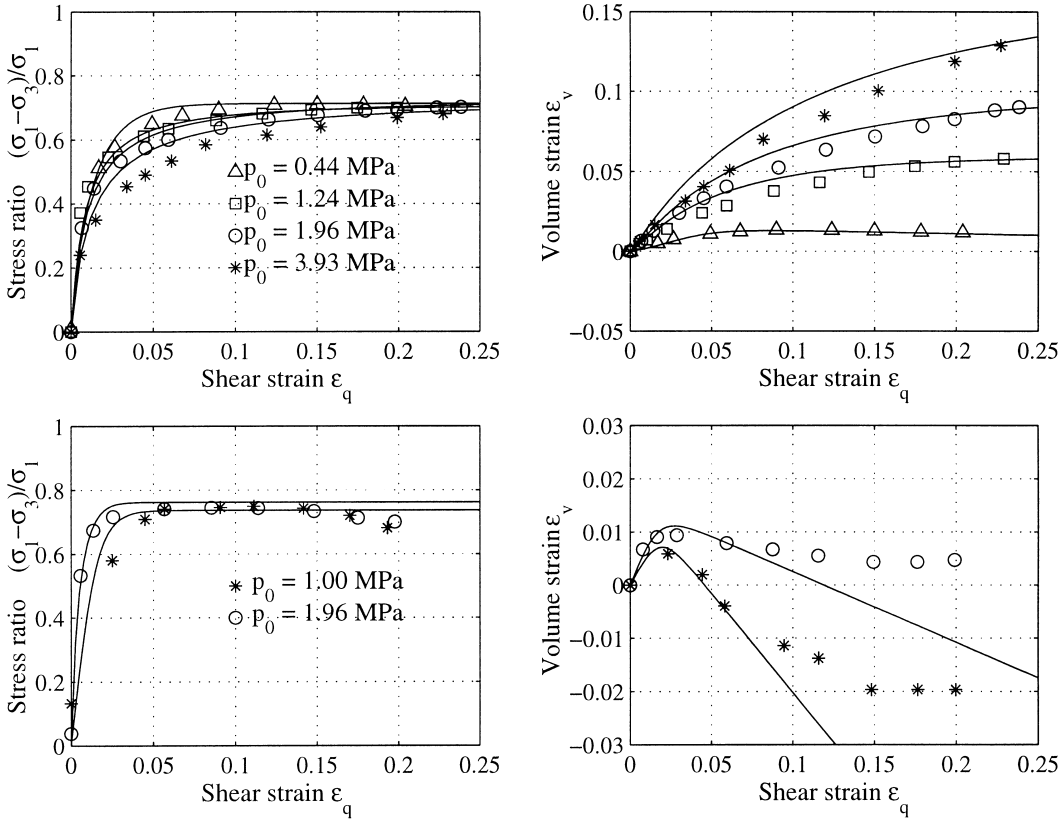

Fig. 9. Theoretical and experimental stress ratio and volumetric strain for loose (top) and dense (bottom) Sacramento sand.

other curves $M_u = M_c$ has been used. The high value of M_c around 1.35 for both loose and dense sand leads to $M_f = 1.0$ in all cases.

The mean parameter values from Tables 3 and 4 are now used to predict the stress path in the constant volume tests carried out by Lee and Seed (1967b). The results are shown in Figs. 10 and 11. The agreement is seen to be very good over the full range in spite of the fact that mean parameters were used. A similar comparison between these experimental data and theoretical predictions was made by Lade and Kim (1995). It is remarkable that the present simpler model seems to capture the first curved part better for the loose sand. This part of the curve is strongly dependent on the shape of the plastic flow potential and the results support the simple friction hypothesis used to derive the present flow

Table 4
Material parameters for dense Sacramento sand, $e = 0.61$

p_0 (MPa)	G (MPa)	$\kappa \times 10^2$	$\lambda \times 10^2$	M_c	M_u	M_f
1.00	67.7	0.74	0.87	1.35	1.55	1.0
1.96	128.1	0.97	1.20	1.38	1.45	1.0
mean	97.9	1.38	1.67	1.37	1.50	1.0

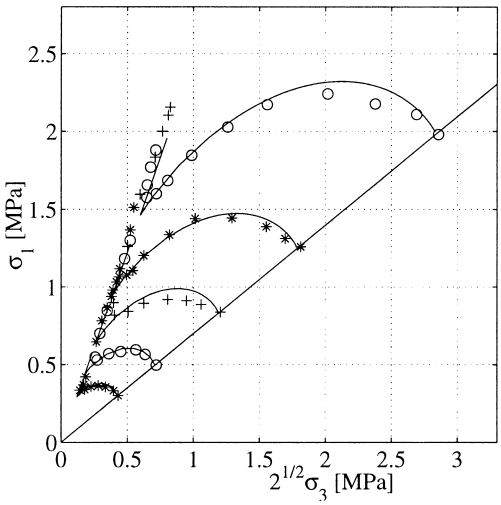

Fig. 10. Constant volume triaxial compression tests with $p_0 = 0.3, 0.5, 0.85, 1.27, 2.0$ MPa on loose Sacramento sand.

potential function (Krenk, 1999). A slight difference between theory and experiments is observed regarding the inclination of the final asymptotic line. This can be ascribed to the uncertainty in the distinction between the parameters κ and M_f in standard triaxial test data, and indeed the asymptotic line in the constant volume test can be used to supply an independent determination of the parameter κ as described in the following.

6.1. The ultimate behaviour in constant volume tests

In the present model the basic characteristics of the stress curves in a constant volume test can be identified explicitly. When the constant volume condition $d\varepsilon_v = 0$ is inserted into Eq. (19), the following

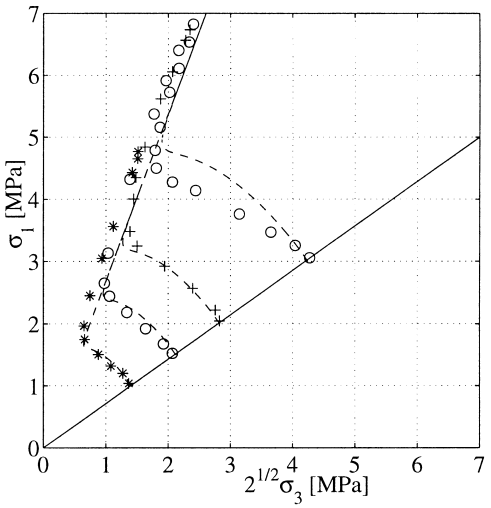

Fig. 11. Constant volume triaxial compression tests with $p_0 = 1.0, 1.5, 2.0, 3.0$ MPa on dense Sacramento sand.

stress increment relation is obtained.

$$\begin{bmatrix} \mathrm{d}p \\ \mathrm{d}q \end{bmatrix} = \left(\begin{bmatrix} 0 \\ 3G \end{bmatrix} - \frac{3G\dfrac{\partial f}{\partial q}}{H + \dfrac{\partial g}{\partial p}K_{\mathrm{e}}\dfrac{\partial f}{\partial p} + \dfrac{\partial g}{\partial q}3G\dfrac{\partial f}{\partial q}} \begin{bmatrix} K_{\mathrm{e}}\partial g/\partial p \\ 3G\partial g/\partial q \end{bmatrix} \right) \mathrm{d}\varepsilon_{\mathrm{q}} \tag{34}$$

It follows from this relation that $\mathrm{d}p < 0$ as long as $\partial g/\partial p > 0$, i.e. as long as $(p,\ q)$ is below the characteristic line. The minimum value of p is obtained for $\partial g/\partial p = 0$, occurring at the characteristic line $(q/p)_{\mathrm{c}} = M_{\mathrm{c}}$. After passage of the characteristic line p increases again.

More importantly, the relation (34) can be used to derive a good estimate of the asymptotic behaviour for large values of $(p,\ q)$. The asymptotic behaviour will be characterized by the ratio $(q/p)_{\mathrm{i}} = M_{\mathrm{i}}$. It follows from the previous argument that $M_{\mathrm{i}} > M_{\mathrm{c}}$. A relation between the incompressible asymptote M_{i} and the material parameters is obtained as follows. The asymptote is described in terms of the ratio q/p which in turn is determined by the ratio of the stress increments $\mathrm{d}q/\mathrm{d}p$,

$$\frac{q}{p} \simeq \frac{\mathrm{d}q}{\mathrm{d}p} = -\frac{H + \dfrac{\partial g}{\partial p}K_{\mathrm{e}}\dfrac{\partial f}{\partial p}}{\dfrac{\partial g}{\partial p}K_{\mathrm{e}}\dfrac{\partial f}{\partial q}} \tag{35}$$

In this relation the elastic bulk modulus $K_{\mathrm{e}} = p/\kappa$ is introduced, leading to the equation

$$\kappa H + \frac{\partial g}{\partial p}\left(p\frac{\partial f}{\partial p} + q\frac{\partial f}{\partial q} \right) = 0 \tag{36}$$

The expression in parentheses is evaluated from the yield function Eq. (6), by using that except for the function $\eta(p)$ the function $f(p, q)$ is homogeneous of degree three in the stresses,

$$\left(p\frac{\partial f}{\partial p} + q\frac{\partial f}{\partial q} \right) = p^4\frac{\mathrm{d}\eta}{\mathrm{d}p} + 3f(p, q) = mp^3\eta \tag{37}$$

When this result is introduced into Eq. (36) together with $H = H_1H_2$ from Eqs. (14) and (18), the equation takes the form

$$\mathscr{F}(M) = \frac{\partial g/\partial p}{\partial g/\partial q} + \eta^{\frac{1}{m}}\frac{\kappa}{\lambda - \kappa}\left(\frac{\partial g/\partial p}{\partial g/\partial q} + w\frac{q}{p} \right) = 0 \tag{38}$$

The parameter M_{i} of the incompressible asymptote is the root of the equation $\mathscr{F}(M_{\mathrm{i}}) = 0$.

The equation $\mathscr{F}(M_{\mathrm{i}}) = 0$ is non-linear and does not have a simple exact solution. However, a simple approximate solution can be found from linear interpolation between the values of $\mathscr{F}(M)$ at the characteristic and ultimate lines, $\mathscr{F}(M_{\mathrm{c}}) > 0$ and $\mathscr{F}(M_{\mathrm{u}}) < 0$. These function values are particularly simple, and as it turns out $M_{\mathrm{c}} < M_{\mathrm{i}} < M_{\mathrm{u}}$. At the characteristic line $\partial g/\partial p = 0$,

$$\mathscr{F}(M_{\mathrm{c}}) = \eta_{\mathrm{c}}^{\frac{1}{m}}\frac{\kappa}{\lambda - \kappa}wM_{\mathrm{c}} > 0 \tag{39}$$

At the ultimate line the hardening $H = 0$ and thereby the term in the parenthesis vanishes. This implies $(\partial g/\partial p)/(\partial g/\partial q) = -w(q/p)_{\mathrm{u}}$, and thus

$$\mathscr{F}(M_u) = -wM_u < 0 \tag{40}$$

Linear interpolation of the function $\mathscr{F}(M)$ between these values gives the root M_i by the relation

$$\frac{M_i - M_c}{M_u - M_i} = -\frac{\mathscr{F}(M_c)}{\mathscr{F}(M_u)} > 0 \tag{41}$$

This equation places the incompressible asymptote M_i between the characteristic line M_c and the ultimate line M_u.

Insertion of the function values and rearrangement of the relation gives the relation in the final form

$$\frac{K_e}{K_p} = \frac{\lambda - \kappa}{\kappa} \simeq \frac{M_u - M_i}{M_i - M_c}\frac{M_c}{M_u}\eta_c^{\frac{1}{m}} \tag{42}$$

In this formula the value of the shape function η at the characteristic line $q/p = M_c$ follows from the yield condition $f(p, q) = 0$,

$$\eta_c = 1 - 3\left(\frac{1}{3}M_c\right)^2 + 2\left(\frac{1}{3}M_c\right)^3 \tag{43}$$

Thus, the ratio between elastic bulk stiffness and its plastic counterpart has been determined in terms of the three parameters M_c, M_u and M_i, all observable directly from standard tests. It is seen that for materials with only a slight change in stiffness due to plasticity, $\lambda \simeq \kappa$, the incompressible asymptote is close to the ultimate line, $M_i \simeq M_u$. Conversely, for materials where plastic deformations are dominating, $\lambda \gg \kappa$, the incompressible asymptote is close to the characteristic line, $M_i \simeq M_c$.

6.2. Adjusting the parameters κ, G and M_f

In the stress plots in Figs. 10 and 11 the characteristic, ultimate and asymptotic incompressible lines are given by

$$\sigma_1 = \frac{3 + 2M}{3 - M}\sigma_3 \quad M = M_c,\ M_u,\ M_i \tag{44}$$

When the parameter M_i is determined from the constant volume data, Eq. (42) gives an equation for the elastic parameter κ, previously determined via an assumed value of M_f. For the dense Sacramento river sand shown in Fig. 11 $M_i = 1.50$. This indicates that $M_u > 1.50$. The most reliable available value of M_u is from the test with $p_0 = 1.00$ MPa, where $M_u = 1.55$. When these values of M_i and M_u are used together with the mean parameters from Table 4, the relation (42) gives the adjusted value $\kappa = 0.0088$. The relation (33b) then gives $G = 95.6$ MPa, and finally $M_f = 0.97$ is found by fitting the location of the final part of the dilation curve to that obtained from the model for the standard triaxial tests. The experimental data are compared with model predictions with the adjusted set of parameters in Fig. 12.

The adjustment of the parameters κ, G and M_f does not influence the fit of the standard triaxial data. In view of the moderate adjustment and the considerable variation of the stiffness data obtained in standard triaxial tests the conclusion in the current case is, that the original estimate of the yield surface parameter M_f by Eq. (25) is quite adequate.

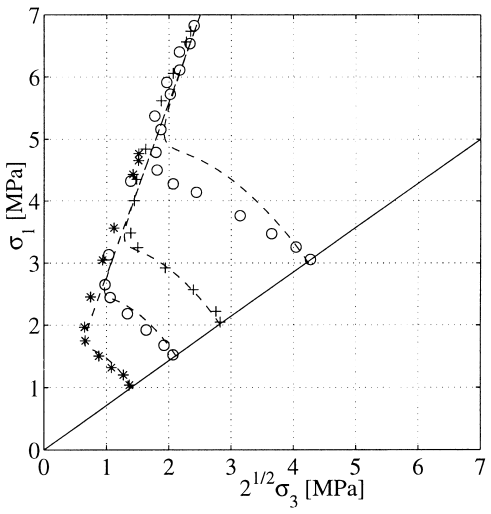

Fig. 12. Undrained triaxial compression tests at different cell pressure on dense Sacramento sand.

7. Conclusions

A calibration procedure has been developed for the elasto–plastic model of granular materials presented by Krenk (1999). This model has a rather small number of parameters, namely the three stiffness parameters G, κ and λ, and the three parameters M_c, M_u and M_f. The calibration procedure is based on stress and strain data available from a standard triaxial test. Five characteristics of the triaxial test data are used directly in calibration: the two initial stress–strain ratios at the start of the application of excess axial stress, the characteristic point of transition from incremental compression to dilation, and the slope and location of the final asymptotic relation between volumetric and shear strain. In this procedure it was used, that the flow potential has an apex at the hydrostatic axis, as demonstrated e.g. by the generalized Coulomb friction theory presented by Krenk (1998). It was demonstrated that the elastic volume flexibility parameter κ and the yield function shape parameter M_f are approximately linearly dependent with respect to the data from a standard triaxial test, and a simple estimate for M_f in terms of the explicitly calibrated parameters M_c and M_u was proposed.

The model gives an excellent representation of the test data, when calibrated by the proposed procedure. However, the simple assumptions from the original Cam–Clay theory regarding elastic properties leads to a systematic change of elastic parameters κ and G with the stress level of the test. As expected, the shear modulus shows an increase with mean stress level, while the tangent bulk modulus should have an increase which is less than linear in the mean stress. This may easily be incorporated in the model, e.g. by deriving the elastic properties from a complementary elastic energy, that is a function of a stress invariant of the form $\frac{1}{2}p^2 + \beta J_2$. This would lead to isotropic secant elastic properties and tangent properties with stress induced anisotropy. While the elastic parameters would gain validity over a wider range of stress conditions by such an extension, the more basic issue that the elastic properties should depend on the plastic deformations, such as changes in void ratio, would require a more fundamental approach to the representation of elastic deformation.

The elasto-plastic model has also been used to discuss the qualitative behaviour of constant volume triaxial tests, and to predict specific behaviour of constant volume tests on dense and loose sand from a previous standard calibration. The material behaviour in the test has two stages: first a compression

stage, during which the mean stress decreases, and after reaching the critical state an increase of mean stress, while approaching a state of proportional increase of the stress components. Also in this case the representation of the test data is excellent. Furthermore, the theory leads to a simple expression for the ratio between the stress components in the final asymptotic stage, from which an improved estimate of the last parameter M_f can be obtained. In the cases investigated the need for an improved value of M_f was marginal.

Acknowledgements

Financial support from the Swedish Technical Research Council is gratefully acknowledged.

References

Andersen, A.T., Madsen, E.B. and Schaarup-Jensen, A.L. (1997), Constitutive modeling in soil mechanics, Masters thesis, Building Technology and Structural Engineering, Aalborg University, Denmark.

Borup, M., Hedegaard, J., 1995. Data Report 9403, Baskarp Sand No. 15. Geotechnical Engineering Group, Aalborg University, Denmark.

Ibsen, L.B., Jakobsen, F.R., 1996. Data Report, Lund Sand No 0, Part 1 and Part 2. Aalborg University, Denmark.

Krenk, S., 1996. A family of invariant stress surfaces. Journal of Engineering Mechanics 122, 201–208.

Krenk, S., 1998. Friction, dilation and plastic flow potential. In: Herrmann, H.J., Hovi, J.-P., Ludig, S. (Eds.), Physics of Dry Granular Media. Kluwer, Dordrecht, pp. 255–260.

Krenk, S., 1999. Characteristic state plasticity for granular materials, Part 1: Basic theory. International Journal of Solids and Structures 37, 6343–6360.

Lade, P., Kim, M.K., 1995. Single hardening constitutive model for soil, rock and concrete. International Journal of Solids and Structures 32, 1963–1978.

Lade, P., Nelson, R.B., 1987. Modelling the elastic behaviour of granular materials. International Journal for Numerical and Analytical Methods in Geomechanics 11, 521–542.

Lee, K.L., Seed, H.B., 1967a. Drained strength characteristics of sand. Journal of the Soil Mechanics and Foundation Division, ASCE 93, 117–141.

Lee, K.L., Seed, H.B., 1967b. Undrained strength characteristics of sand. Journal of the Soil Mechanics and Foundation Division, ASCE 93, 333–360.

Schofield, A.N., Wroth, C.P., 1968. Critical State Soil Mechanics. McGraw-Hill, New York.